# Distinct element method analysis and field experiment of soil resistance applied on the subsoiler

Li Bo, Liu Fanyi, Mu Junying, Chen Jun*, Han Wenting

(*College of Mechanical and Electronic Engineering, Northwest A & F University*, *Yangling, Shaanxi* 712100, *China*)

**Abstract:** Since the design of the subsoiler is a complex work, the interaction between the subsoiler and soil was investigated by using Distinct Element Method (DEM) in this study. Based on the traditional discrete element theory, the 3D model of soil particles and the subsoiler were established after considering the liquid bridge force between soil particles. The operating resistance curves of the subsoiler were achieved after the DEM simulation at a speed of 1 m/s, and three depths of 180 mm, 220 mm and 260 mm, respectively. The simulation curves agreed well with the field experimental results based on relative errors of 2.96%, 14.95% and 7.15%, respectively, at three depths. All these data proved that it was feasible and favorable to analyze the performance of the subsoiler by using the DEM and it is of important significance for studying and further optimizing the structure of the subsoiler.

**Keywords:** distinct element method (DEM), parallel bond, subsoiler, modeling, simulation

**DOI:** 10.3965/j.ijabe.20140701.006

**Citation:** Li B, Liu F Y, Mu J Y, Chen J, Han W T. Distinct element method analysis and field experiment of soil resistance applied on the subsoiler. Int J Agric & Biol Eng, 2014; 7(1): 54－59.

## 1 Introduction

Subsoiling can greatly improve the growing environment of crops and increase utilization rate of soil nutrients[1]. The design and manufacture of the subsoiler are of great significance because it has a direct impact on subsoiling effects. The working process of the subsoiler is the interaction with a large number of soil particles so it needs to have less resistance to save power consumption and a good ripper effect. Therefore, the interaction between soil particles and the subsoiler needs to be considered in the analysis. Many researchers have tried some ways[2,3] to optimize the subsoiler, while tedious trials are needed and it is difficult to obtain a satisfactory design.

In recent years, many researchers carried out related studies using the finite element method[4-7]; however, the movement of soil particles and the cracking and deformation of the soil during the process of tillage cannot be modeled using finite element method mainly dealing with continuum so it cannot analyze the working process of the subsoiler well. As a method of analyzing the motion of particles, distinct element method (DEM) breaks the limit of seeing soil as a continuum and it provides a new way of thinking in the study of the interaction between the subsoiler and soil.

The DEM was first proposed by Cundall and Strack[8] as a method of analyzing the motion of particles. The force and motion of particles were determined by the static contact force between particles and Newton's laws. The application of DEM has an important significance for the study of working process of agricultural machinery. In recent years, Tsuji et al.[9] used a cohesive bond force model proposed by Utili and Nova[10] to study the motion

**Received date:** 2013-09-16 **Accepted date:** 2014-02-09

**Biographies: Li Bo,** PhD student, Research focuses on agricultural Engineering, Email: 1061328564@qq.com. **Liu Fanyi,** Master student, Research focuses on agricultural Engineering, Email: 1017856727@qq.com. **Mu Junying,** Master student, Research focuses on agricultural Engineering, Email: 459446509@qq.com. **Han Wenting,** PhD, Professor, Research focuses on agricultural electrification and automation, Tel: 029-87091325, Email: hanwt2000@126.com.

***Corresponding author: Chen Jun,** PhD, Professor, Northwest A & F University, Yangling, Shaanxi 712100, China; Tel: 029-87091867, Email: chenjun_jdxy@nwsuaf.edu.cn.

of particles. Shmulevich et al.[11] used the method proposed by Asaf et al.[12] in 2007 to determine the mesoscopic parameters of the soil and compared the operating resistance of four blade cross-section shapes. Zhang et al.[13,14] developed a bionic bulldozing plate and analyzed the working process of the bulldozing plate using DEM. Yu et al.[15] compared two types of furrow openers. The operating process and resistance in three kinds of soils with different moisture contents at three different velocities and depths were analyzed and proved that it was feasible to analyze the performances of furrow openers by using the DEM. Obermayr et al.[16] studied the interaction between the unbonded soil particles and the bulldozing plate. Shmulevich[17] reviewed and summarized the simulation methods used in the bulldozing plate working process. Chen et al.[18] added bond force to particles and simulated the working process of the subsoiler in three different soils through changing particle stiffness.

At present, the working parts of agricultural machinery models are established oversimplified in many studies[11-16] because they are usually 2D models, which are far from the actual situation and would lead to inaccurate simulation. Many models of soil only consider the contact force and friction between particles and the influence of adhesion are not taken into account, or the cohesive effect only acts at the contact point, ignoring the rotation restriction between the particles. In addition, the liquid bridge force caused by the soil moisture has a nonnegligible effect on the interaction among the soil particles so it must be considered.

A precise 3D model of subsoiler was established in this paper. The 3D nonlinear model of soil particles was established and the parallel bond was added to the model for simulating the liquid bridge force. Discrete element analysis software Particle Flow Code in 3D (PFC3D) was used in the study to simulate the working process of the subsoiler.

## 2 Materials and methods

### 2.1 Experiment in the filed

An arc-shaped subsoiler was chosen in the experiment, which was carried out on a test field in Northwest A & F University, Yangling, Shaanxi, China. The test field was a wheat stubble land (30 m in length and 30 m in width), which was the general working environment of the subsoiler. The farming area was 25 m in length and the soil moisture content was 19% (weight percentage), and the porosity was 0.4 (tested in the lab). The test platform was a Foton 4040 tractor (Foton heavy industries CO., LTD, Shandong, China). Sensors used in the experiment consisted of an upper link sensor of CYB-602S and left (right) hanging pin sensors of CYB-601S. The dynamic data collector was installed on the tractor.

The subsoiler was set to work at 1 m/s and three depths of 180 mm, 220 mm and 260 mm, depending on the operating requirements in China[19]. Before conducting the experiment, the subsoiler should be adjusted to the specified depth at first then started the dynamic data collector. The experiment could be started under 1 m/s after the tractor worked. Sensors transmitted sampling data to the dynamic data collector then the data emitted from the built-in wireless transmitting device of SZ02-USB-2K. The data were collected by a receiving antenna installed on the laptop which was not far away from the field and then the telemetry acquisition program transformed the data into the operating resistance of the subsoiler. Instruments used in the experiment were shown in Figure 1. The experiment was repeated twice at each depth.

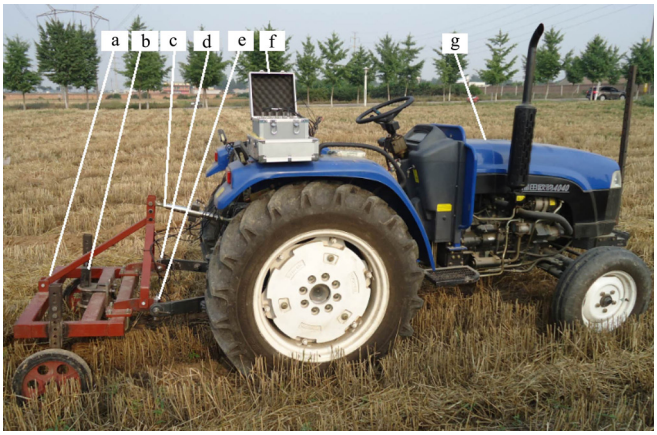


Note: a: rack; b: the subsoiler; c: upper link sensor of CYB-602S; d: left hanging pin sensor of CYB-601S; e: right hanging pin sensor of CYB-601S; f: dynamic data collector; g: Foton4040 tractor

Figure 1 Instruments used in the experiment

### 2.2 Modeling

#### 2.2.1 Model of the subsoiler

Establishing the model accurately is very critical for

the analysis of the working process of the subsoiler. In this study, the 3D model of the subsoiler was established by 3D modeling software Pro/Engineer (PROE) which was commonly used in designing and developing products and the size ratio was 1:1 compared with the actual subsoiler. This model was shown in Figure 2.

2.2.2 Model of the soil particles

In the natural state, soil is made up of solid soil particles, soil moisture and the air existing in the soil pore, therefore, it is inaccurate enough to regard the soil as solid soil particles. Soil moisture plays an important role in the interaction among the soil particles. The types of soil moisture are hygroscopic water, membrane water, capillary water and gravity water[13,14], and capillary water has the highest impact on the force among soil particles in forms of liquid bridge (Figure 3).

Figure 2 Model of the subsoiler

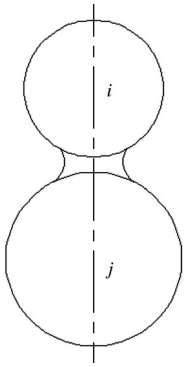


Figure 3 Effect of liquid bridge on the force among soil particles

The 3D soil particles model was established in this paper. Since the shape of the soil particle was nearest to a ball, it was considered as an ideal ball (Figure 4). For the two contact particles, the force between them can be divided into the normal force $N$ and tangential force $T$.

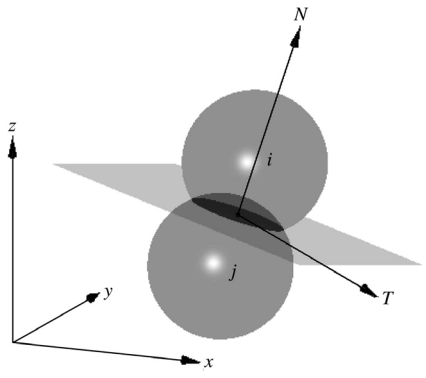


Figure 4 Particle effect of 3D ball model

Based on the traditional discrete element model established by Cundall[4], in addition to considering the contact force and friction among soil particles, parallel bond was added to represent the liquid bridge between particles. Figure 5 shows the contact model of two soil particles, $i$ and $j$. The normal and the shear contact springs represent the contact force; the slider represents friction; the parallel-bond springs represent the parallel-bond effect; the normal and the shear viscous dashpots represent the effects of viscous damping on soil particles.

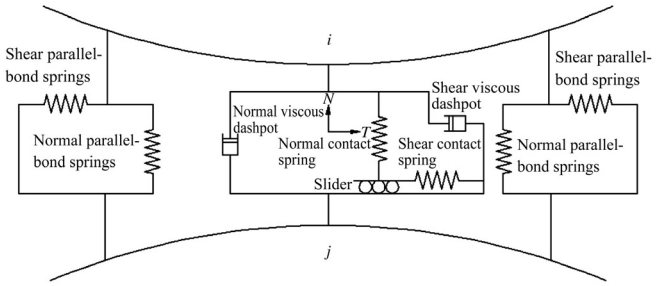


Figure 5 Model of soil particles

According to DEM theory[20], the integrated force calculation equation among the soil particles is:

$$[F]=[F_c]+[F_d]+[F_f]+[F_p]$$

In the formula, $[F]$ is the integrated force including the total resultant force and the total moment; $[F_c]$ is the sum of contact force among soil particles (including normal force and shear force) and the moment; $[F_d]$ is the sum of viscous damping force (including normal force and shear force) and the moment; $[F_f]$ is the friction; $[F_p]$ is the parallel-bond force (including normal force and shear force) and the moment.

Parallel bond can either transfer the force or the moment. A parallel bond can be simplified as a normal spring and a shear spring. Relative motion at the contact (occurring after the parallel bond has been created) causes a force and a moment to develop within the bond material as a result of the parallel-bond stiffness. This force and moment act on the two bonded particles and can be related to maximum normal and shear stresses acting within the bond material at the bond periphery. If either of these maximum stresses exceeds its corresponding bond strength, the parallel bond would break. $[F_c]$ and $[F_d]$ act on the contact point of two particles while the

parallel bond distributed over a circular disk lying on the contact plane and centered at the contact point.

### 2.3 Determination of the mesoscopic parameters

The mesoscopic parameters of soil particles are particularly critical for the simulation and they cannot be measured through physical test directly. In this study, the SJ-1A triaxial shear apparatus (Figure 6) was used to obtain the stress-strain curve under the unconsolidated-undrained condition.

Figure 6 SJ-1A triaxial shear apparatus

### 2.4 Simulation

In order to simulate the working process of subsoiler, a soil bin of 1 m long, 0.5 m wide and 1 m high was built. 3D soil particles were generated using the model mentioned above before importing the model of subsoiler. Set the subsoiler to work at 1 m/s and the specified depth after the soil particles reached equilibrium. The simulation process was shown in Figure 7.

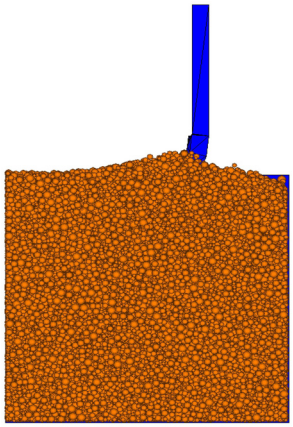

Figure 7 Simulation of working process for the subsoiler using distinct element method

## 3 Results and discussion

Through adjusting the input parameters of DEM repeatedly, the simulation curve was finally brought into correspondence with the stress-strain curve obtained in the laboratory[21,22], as shown in Figure 8 (confining pressure is 50 kPa). The definitive mesoscopic parameters of soil used for DEM simulation were shown in Table 1.

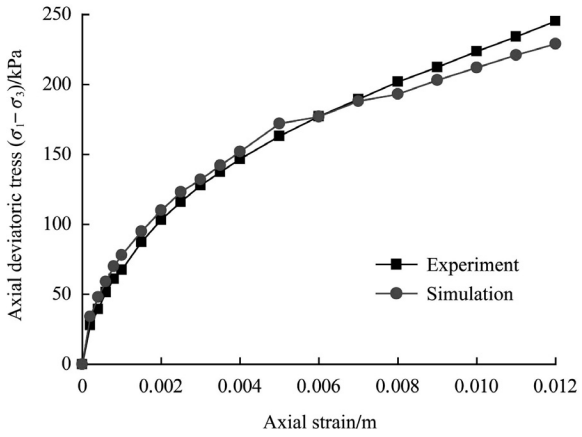


Figure 8 Stress-strain curves in the simulation and laboratory test

**Table 1 Selection of parameters for DEM analysis**

| Parameter | Value |
|---|---|
| Soil porosity | 0.40 |
| The smallest radius of particles /m | 0.0006 |
| Ratio of the largest to the smallest radii of particles | 3 |
| Friction factor | 0.93 |
| The total number of particles | 47 832 |
| Soil particle density /kg·m$^{-3}$ | 2 760 |
| Particle-particle contact normal stiffness /N·m$^{-1}$ | 400 000 |
| Particle-particle contact shear stiffness /N·m$^{-1}$ | 350 000 |
| The critical damping ratio in the normal direction | 0.8 |
| The critical damping ratio in the shear direction | 0.6 |
| The parallel-bond radius multiplier | 1.0 |
| The parallel-bond normal stiffness /Pa·m$^{-1}$ | 1e6 |
| The parallel-bond shear stiffness /Pa·m$^{-1}$ | 1e6 |
| The parallel-bond normal strength /Pa | 1e6 |
| The parallel-bond shear strength /Pa | 1e6 |

Figure 9 is the simulation curve of operating resistance of the subsoiler with a depth of 220 mm and a speed of 1 m/s and Figure 10 shows the average operating resistance curve in double repeated experiment at the same depth and velocity. Other curves under different depths have the same trends with Figure 9 and Figure 10.

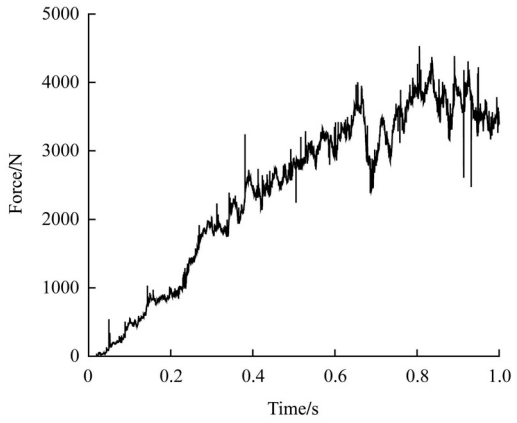


Figure 9 Simulation curves of operating resistance of the subsoiler at 220 mm in depth

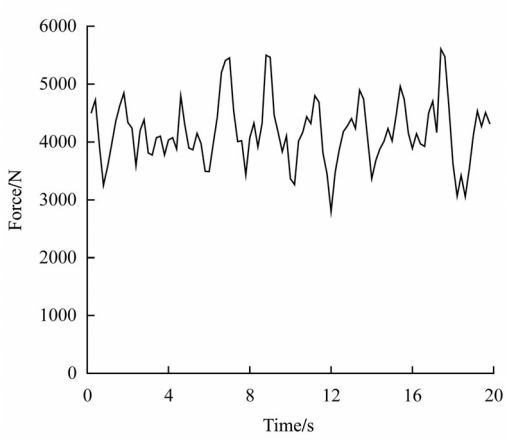


Figure 10 Average operating resistance curves of the subsoiler in double repeated experiment at 220 mm in depth

The subsoiler was set at 220 mm in depth which moved into the soil bin from the right side. As it can be seen from Figure 9, with the subsoiler starting to largely contact with the soil, the resistance increased from 0 and stability reached 0.64 s, so the average force after 0.64 s was selected to calculate the simulation operating resistance. The resistance calculated from the simulation was 3 630 N. The figure showed that the curve fluctuation was small (the range was about 800 N) because soil particles in different size evenly distributed in the soil bin. The reason for the fluctuation was that during the working process, the soil in front of the subsoiler continued to accumulate which led to the increase of the resistance, when the accumulated soil reached a value the soil began to fall then the resistance decreased so the curve would be volatile like this.

Figure 10 shows that there is a relatively large fluctuation (the range was about 2 000 N) in the experiment, this is because the situation is complicated in the field that different regions have great otherness and the data are affected by the wheat's roots. However, the overall resistance in the test region was changed within a certain range and the average working resistance of the subsoiler measured by the sensors was 4 268 N.

With the fixed operating speed of 1 m/s, average operating resistance of the subsoiler and the relative errors were shown in Table 2, based on tillage depth of 180 mm, 220 mm and 260 mm, respectively.

**Table 2 Tillage resistance of the subsoiler in different depths**

| Depth /mm | Resistance in experiment/N | Resistance in simulation/N | Relative errors/% |
|---|---|---|---|
| 180 | 2 834 | 2 750 | 2.96 |
| 220 | 4 268 | 3 630 | 14.95 |
| 260 | 5 428 | 5 040 | 7.15 |

It can be seen from Table 2 that the tillage resistances obtained by the DEM simulation are close to that of the experiment, but all the results are smaller than the value measured in the experiment. This is due to the wheat roots which increase the working resistance of the subsoiler. As it can be seen, the relative errors are relatively small, with minimum of 2.96% and maximum 14.95%, indicating that the DEM can simulate the working process of the subsoiler well and the result has a very good reference value for the actual situation because of the complicated condition in the field.

The simulation still had a bit of room for improvement, for example, the simulation was completed in a soil bin of 1 m long, 0.5 m wide and 1 m high, so the rigid walls would have a certain effect on the tillage resistance which was different from the actual situation[23]. In addition, the effect of wheat roots was not considered in the modeling. All these are needed to be improved in future.

## 4 Conclusions

1) A precise 3D model both for the subsoiler and soil particles was developed in this study. With the liquid bridge force taken into account, the parallel bond was added.

2) The subsoiler working process was simulated by using discrete element software (PFC3D) at speed of 1 m/s, and three depths of 180 mm, 220 mm and 260 mm, respectively. By comparing the simulation tillage

resistance results with the experimental data in the field, the relative errors were 2.96%, 14.95% and 7.15%, respectively. All these data proved that it was feasible to analyze the working process of the subsoiler by using the DEM.

3) This study will lay a foundation for analyzing the resistance of the subsoiler in the future and improving its structure by comparing the optimized subsoiler with existing subsoilers on resistance. It may provide designers a useful method to improve subsoilers.

## Acknowledgements

This study was funded by the National Science and Technology Supporting Plan (No. 2011BAD29B08) and the "111"Project (No. B12007).

## [References]

[1] Guo Z J, Tong J, Zhou Z L, Ren L Q. Review of subsoiling techniques and their applications. Transactions of the CSAE, 2001; 17(6): 169-173. (in Chinese with English abstract)

[2] Miszczak M. A torque evaluation for a rotary subsoiler. Soil & Tillage Research, 2005; 84(2): 175-183.

[3] Shahgoli G, Fielke J, Saunders C, Desbiolles J. Simulation of the dynamic behaviour of a tractor-oscillating subsoiler system. Biosystems Engineering, 2010; 106(2): 147- 155.

[4] Mouazen A M, Ramon H. A numerical-statistical hybrid modelling scheme for evaluation of draught requirements of a subsoiler cutting a sandy loam soil, as affected by moisture content, bulk density and depth. Soil & Tillage Research, 2002; 63(3): 155-165.

[5] AboElnor M, Hamilton R, Boyle J T. Simulation of soil-blade interaction for sandy soil using advanced 3D finite element analysis. Soil & Tillage Research, 2004; 75(1): 61-73.

[6] Mouazen A M, Nemenyi M. Finite element analysis of subsoiler cutting in non-homogeneous sandy loam soil. Soil & Tillage Research, 1999; 51(1): 1-15.

[7] Zhang Q, Zhang L, Yu H Y, Xiao Y K. Finite element analysis and experiment of soil resistance of multiplex-modality subsoiler. Transactions of the CSAM, 2012; 43(8): 61-65. (in Chinese with English abstract)

[8] Cundall P A, Strack O D L. A discrete numerical model for granular assembles. Géotechnique, 1979; 29(1): 47-65.

[9] Tsuji T, Nakagawa Y, Matsumoto N, Kadono Y, Takayama T, Tanaka T. 3-D DEM simulation of cohesive soil-pushing behavior by bulldozer blade. Journal of Terramechanics, 2012; 49(1): 37-47.

[10] Utili S, Nova R. DEM analysis of bonded granular geomaterials. International Journal for Numerical and Analytical Methods in Geomechanics, 2008; 32(17): 1997-2031.

[11] Shmulevich I, Asaf Z, Rubinstein D. Interaction between soil and a wide cutting blade using the discrete element method. Soil & Tillage Research, 2007; 97(1): 37-50.

[12] Asaf Z, Rubinstein D, Shmulevich I. Determination of discrete element model parameters required for soil tillage. Soil & Tillage Research, 2007; 92(1): 227-242.

[13] Zhang R, Li J Q, Zhou C H, Xu S C. Simulation of dynamic behavior of soil ahead of the bulldozing plates with different surface configurations by discrete element method. Transactions of the CSAE, 2007; 23(9): 13-19. (in Chinese with English abstract)

[14] Zhang R, Chen B, Li J Q, Xu S C. DEM simulation of clod crushing by bionic bulldozing plate. Journal of Bionic Engineering (Supplement), 2008; 5: 72-78.

[15] Yu J Q, Qian L B, Yu W J, Pan S Q, Fang Y, Fu H. DEM analysis of the resistances applied on furrow openers. Transactions of the CSAE, 2009; 40(6): 53-57. (in Chinese with English abstract)

[16] Obermayr M, Dressler K, Vrettos C, Eberhard P. Prediction of draft forces in cohesionless soil with the Discrete Element Method. Journal of Terramechanics, 2011; 48(5): 347-358.

[17] Shmulevich I. State of the art modeling of soil-tillage interaction using discrete element method. Soil & Tillage Research, 2010; 111(1): 41-53.

[18] Chen Y, Munkholm L J, Nyord T. A discrete element model for soil–sweep interaction in three different soils. Soil & Tillage Research, 2013; 126: 34-41.

[19] He J, Li H W, Gao H W. Subsoiling effect and economic benefit under conservation tillage mode in Northern China. Transactions of the CSAE, 2006; 22(10): 62-67. (in Chinese with English abstract)

[20] PFC3D (Particle Flow Code in 3 Dimensions) Manual, Version 3.0, Itasca Consulting Group, Inc., Minneapolis, MN, USA, 2002.

[21] O'Sullivan C, Cui L. Micromechanics of granular material response during load reversals: combined DEM and experimental study. Powder Technology, 2009; 193(3): 289- 302.

[22] Belheine N, Plassiard J P, Donze F V, Darve F, Seridi A. Numerical simulation of drained triaxial test using 3D discrete element modeling. Computers and Geotechnics, 2009; 36(1): 320-331.

[23] Li Y J, Liu J H, Xu Y. Discrete element simulations of the cone penetration tests in sandy Soil. Transactions of the CSAM, 2011; 42(12): 44-48. (in Chinese with English abstract)